Journal of Mines, Metals and Fuels, *72(2): 93-102; 2024. DOI: 10.18311/jmmf/2024/36429*

Print ISSN : 0022-2755

Journal of Mines, Metals and Fuels

Contents available at: *www.informaticsjournals.com/index.php/jmmf*

Selective Laser Melting of AlSi10Mg: Corrosion Behavior

Prabhukumar Sellamuthu[1]*, Katakam Sivaprasad[2] and Konda Gokuldoss Prashanth[3,4]

[1]Department of Mechanical Engineering, Presidency University, Bengaluru – 560064, Karnataka, India; prabhukumar.sellamuthu@gmail.com

[2]Advanced Materials Processing Laboratory, Department of Metallurgical and Materials Engineering, National Institute of Technology, Tiruchirappalli – 620015, India

[3]Department of Mechanical and Industrial Engineering, Tallinn University of Technology, 19086 Tallinn, Es-tonia

[4]Centre for Biomaterials, Cellular and Molecular Theranostics, Vellore Institute of Technology, Vellore – 632014, Tamil Nadu, India

Abstract

Additive Manufacturing (AM) processes can theoretically fabricate materials with any complex structures with added functionality at low costs. However, the properties of components developed by AM should not lose to the properties observed in components fabricated through conventional manufacturing methods. In this study, the corrosion resistance of AlSi10Mg alloy processed through Selective Laser Melting (SLM) in contrast to its tra-ditional counterpart, Sand-Casting (SC) was investigated. Potentiodynamic polarization tests were performed to study the electrochemical behaviour in a 3.5% NaCl solution. It was observed that the corrosion resistance of the SLM material is relatively better than the SC alloy under similar test conditions. It may be concluded that the unique solidification conditions existing during the SLM process may lead to marginally improved corrosion resistance in the alloy considered.

Keywords: *Additive Manufacturing, AlSi10Mg Alloy, Corrosion, Selective Laser Melting*

1.0 Introduction

Additive Manufacturing (AM) has become the potential technology to fabricate components with intricates using almost all varieties of engineering materials[1,2], including crystalline materials (Al-, Ag-, Co-, Cu-, Fe-, Ni-, Ti-, etc.)[3-25], amorphous materials (bulk metallic glasses)[11,26,27], quasicrystalline materials[28], high entropy alloys[29-31], and composites[32-36]. Among the different AM processes, Selective Laser Melting (SLM) also known as the Laser Powder-Bed Fusion Process (LPBF) is the most progressing and widely used technology in which the components are manufactured layer-by-layer where the powder-bed is scanned by a high-power laser beam (source) as governed by a CAD model[37-39]. The corrosion behaviour of SLM-fabricated alloy significantly influences the parts in their service conditions, especially in the aerospace, automobile, marine, oil, and pipeline industries, etc., It is vital to study the effect of various metallurgical features present in the microstructure, especially in the point of view of corrosion properties[40]. AlSi10Mg alloy[41,42] and AlSi12 alloy[43-45] are the most widely fabricated Al-based alloys using the SLM process. Al-based alloys containing Si (which imparts fluidity) are extensively utilized because of their low melting point/solidification range, low shrinkage, and good castability[46,47]. AlSi10Mg

*Author for correspondence

alloys (particularly hypoeutectic) are used in above mentioned industries because of their low coefficient of thermal expansion, low density, and high specific strength[48].

The microstructure of AlSi10Mg alloy consists of an α-phase containing Al, a β-phase like Mg_2Si, and a eutectic Al-Si mixture. Previous studies show that the presence of coarse and acicular eutectic Si particles deteriorates the mechanical properties of AlSi10Mg alloy[49-51]. Hence, the mechanical properties of AlSi10Mg alloy can be improved by modifying its microstructure (especially the morphology of the Si particles)[51]. A finer microstructure with homogenized eutectic Si particles in the Al matrix could be obtained through a rapid solidification process like SLM[52,53]. On the contrary, the cooling rate in conventional casting is much less when compared to the SLM process[54]. So, a finer microstructure with homogenized eutectic Si particles in the Al matrix could be obtained through SLM[55]. The commercial applications of SLM-processed materials depend also on their corrosion properties[56]. Earlier investigations reveal that the corrosion resistance of additive-manufactured Al-based alloys is higher than its conventional cast counterpart[57] due to homogenized microstructure and the absence of Fe-based intermetallics[56]. On the other hand, some other researchers have observed poor corrosion resistance because of passive layer malfunctioning[56,58]. The friction stir processing of SLM-fabricated AlSi10Mg results in a change in pitting potential and a reduction in corrosion rate and corrosion current density thereby enhancing its corrosion properties[59]. Some other researchers have also reported similar corrosion resistance for the AlSi10Mg alloy produced by both conventional casting and SLM[60]. Some researchers have demonstrated that the corrosion properties of the SLM-fabricated AlSi10Mg alloy could be improved through a suitable heat treatment process by removing any internal stresses formed during rapid solidification and achieving uniform distribution of eutectic Si particles in the Al matrix[61]. However, Kubacki *et al.*[62] and Gu *et al.*[63] observed a reduced corrosion performance in heat-treated AlSi10Mg alloys fabricated by SLM.

The reports on the corrosion behaviour of AlSi10Mg fabricated by SLM are mixed in nature, where some researchers have shown improved corrosion properties as compared to their cast counterparts and others demonstrated either similar or inferior properties for SLM-processed material[41,42,61,64]. Hence, the present work is of utmost significance as it discusses the corrosion behaviour of SLM-processed AlSi10Mg alloy by potentiodynamic polarization tests and the results are compared with their counterpart (sand-cast AlSi10Mg alloy). It is hypothesized in this work that the corrosion resistance of SLM-processed AlSi10Mg alloy will be better than its cast counterpart due to its refined microstructure.

2.0 Materials and Methods

2.1 Sample Preparation

The AlSi10Mg samples were fabricated by SLM using the EOSINT M280 system with the standard process parameters: 200 W laser power, 500 mm/s scanning speed, 30 µm layer thickness, and 0.125 mm hatch spacing. Both cylindrical specimens and rectangular specimens were fabricated according to the ISO/ASTM 52921-13 standard. Metallic powders were used as feedstock material with a particle size of ~50 µm under a pure argon gas protective atmosphere. The SLM-processed samples were stress-relieved using annealing heat treatment at 300°C for 2 h in a muffle furnace (Delta Power/2019). The cast counterparts were produced by remelting Al alloy

Table 1. Chemical composition of the Selective Laser Melted (SLM) and Sand-Cast (SC) AlSi10Mg alloys evaluated by optical emission spectrometer

Alloy(wt.%)	Si	Mg	Mn	Fe	Cu	Sn	Ni	Zn	Ti	Pb	Al
SLM	10.16	0.41	0.01	0.31	0.01	0.01	0.19	0.01	0.03	0.01	Bal.
SC	10.82	0.27	0.03	0.34	0.07	0.01	0.02	0.01	0.01	0.01	Bal.

at 680°C in an induction furnace with inherent stirring. Ingots were cast using a sand-casting process employing a rectangular iron die of (100 x 10 x 10) mm^3. The central portion of the ingot was used to prepare test specimens. The chemical composition of the SLM and sand-cast sample are shown in Table 1.

2.2 Microstructural Characterization

The microstructure of the samples was examined by optical microscopy (LEICA DMI8C, Germany) coupled with image analyzer software (ENVISION 6.0) and Scanning Electron Microscopy (SEM) with a GEMINI 300 CARL ZEISS (CARL ZEISS, Germany) provided with spot chemical analysis using an Energy Dispersive Spectroscopy (EDS) detector. SiC emery papers (280, 320, 400, 800) were used to rough grind the sample surfaces. Then the samples were subjected to diamond polishing with a particle size of 5 µm, 3 µm, and 1 µm, respectively. Kallings reagent (33-50 % Ethanol, ~2% Cupric chloride dihydrate, 33-50 % hydrochloric acid, and 0-33% water) was used to etch the samples for microstructural analysis. Samples were exposed to etching reagent for 10 seconds to reveal the microstructures

2.3 Phase Analysis

The internal phases present in the AlSi10Mg samples were identified using X-ray diffractometer ULTIMA IV, RIGAKU (RIGAKU, Tokyo, Japan) with Cu-K_α radiation using the following parameters: 40 kV voltage, 30 mA current, spot size 5 x 5 mm and 2°/min scanning rate. X'pertHighscore Plus software was used to analyze the diffraction peaks.

2.4 Mechanical Testing

The microhardness of the AlSi10Mg samples was measured using the Vickers microhardness tester. Vickers microhardness of the sample was calculated on the longitudinal section of the as-built parts using an Indentec 5030KV microhardness testing machine with a 0.5 kg load and a 10 s dwell time. 3 tests were conducted and the mean value is reported.

2.5 Electrochemical Characterization

The corrosion behaviour was investigated using electrochemical characterization in the form of Potentiodynamic Polarization (PDP) analysis as well as by weight loss tests. The corrosion tests were conducted using a 3.5% NaCl solution with an electrolyte containing naturally dissolved oxygen. The PDP analysis was done with BIOLOGIC SP-150 incorporated with Ec-Lab software V10.44. The tests were conducted using a standard three-electrode cell with a Saturated Calomel Electrode (SCE) as a reference electrode and using 0.5 mV/s scanning rate from -2 V to -0.6 V. This PDP is a preliminary and qualitative method to evaluate the sample.

3.0 Results and Discussion

3.1 Microstructural Analysis

The optical images along the cross-section of the SC and SLM fabricated AlSi10Mg samples are shown in Figure 1 (a)-(c) respectively. The microstructure of the SC AlSi10Mg alloy consists of pro-eutectic Al-dendrites

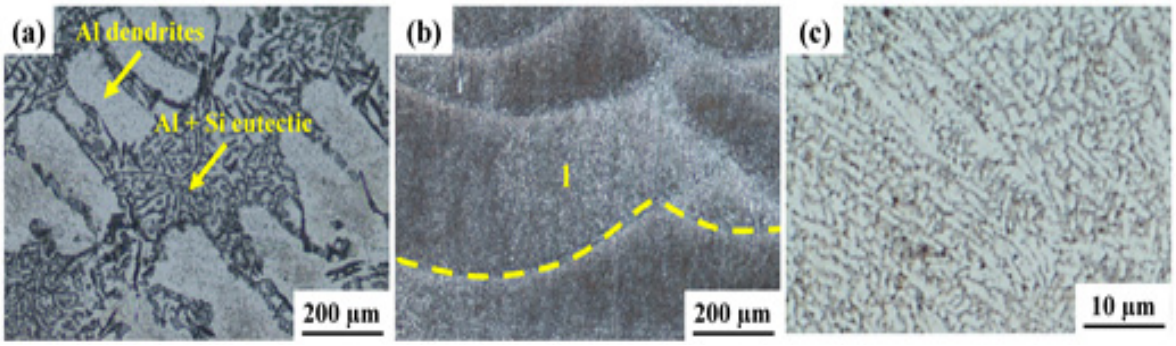

Figure 1. Optical microscopy images of the **(a)** sand-cast and selective laser melting processed AlSi10Mg alloy at **(b)** lower magnification and **(c)** higher magnification.

along with Al-Si eutectics and some porosity. The observed microstructure in Figure 1 (a) is typical for any hypoeutectic composition. It was observed that the solidification rate of SLM-processed AlSi10Mg is comparatively higher than that of its SC counterpart and hence a very fine microstructure is obtained at the same scale. However, the microstructure is difficult to resolve at the length scale considered (Figure 1 (b)). Only features like the laser melting tracks are visible under the length scale considered as highlighted in Figure 1(b). A higher magnification optical image of SLM-fabricated AlSi10Mg is shown in Figure 1(c). The microstructure shows the dendritic features at an excellent scale (in a sub-micron regime) where neither eutectic morphology nor the presence of Si platelets is observed, unlike the cast condition. In short, it may be summarized that the SLM-processed samples do not show a typical hypo-eutectic-like microstructure but a unique morphology. The present results illustrate that the high cooling rates observed during the SLM process lead to refined microstructure features[65,66]. In addition, the unique solidification conditions existing during SLM fabrication lead to variations in the morphology of the microstructure[54].

SEM images of the SC and SLM fabricated AlSi10Mg samples are shown in Figure 2. The microstructure of the SC AlSi10Mg alloy (Figure 2(a)) shows the presence of hypo-eutectic Al dendrites distributed all over the sample. In addition, eutectic Al-Si and some minor precipitates of Fe-Mn are also observed. The magnified images (Figure 2 (b), (c)) show the presence of Si platelets with the presence of some defects like micro-cracks within the Si platelets. In addition, the SC materials show typical casting defects like porosity. In the SLM fabricated samples (Figure 2 (d)-(f)), the melt pool features along with the overlaps present due to successive laser scanning which remelts some parts of the previously solidified layers. The stacking of the melt pool features results due to successive melting and solidification of different layers during the SLM process. The microstructure of the SLM-processed AlSi10Mg alloy (Figure 2 (e), (f)) primarily consists of a cellular microstructure with Al in the core of the cells and Si along the cell boundaries[52]. The Si is not present in the form of particles/platelets but as a

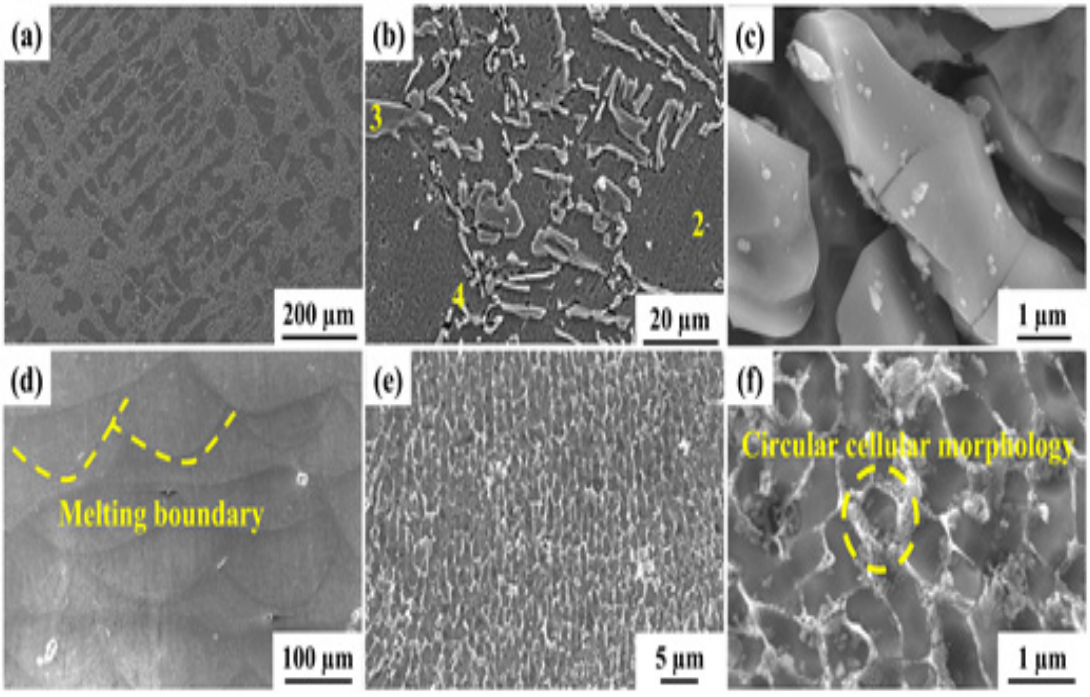

Figure 2. Scanning electron microscopy images of the AlSi10Mg samples fabricated by **(a-c)** sand cast, and **(d-f)** selective laser melting.

continuous phase. It was also observed that the porosity present in the SLM samples is mostly accumulated at the melt pool boundaries, which is typical for the SLM process[67]. The significant differences observed in the microstructures of the AlSi10Mg fabricated by both SC and SLM along the different length scales for the basis for the differences in the different properties observed in these samples including corrosion properties.

3.2 Phase Identification

Figure 3 shows the XRD patterns of both SC and SLM-processed AlSi10Mg alloy. Both the samples show the presence of Al and Si phases, as expected. The intensity for the Al peaks has reversed between (111) and (022) in the SLM condition suggesting the presence of crystallographic texture in the material, which is absent in the SC counterpart. On the other hand, the SC material shows some small traces of the Fe-Mn phase, which is not the case in the SLM condition. Such minor differences in the phase might be due to the minor variations in the trace elements concentration present in these samples that come from the feed-stock material. The peaks are found to be broadened for the SLM samples as compared to the SC counterparts because of the following reasons: (1) high degree of internal stresses, (2) Supersaturation of Si in the Al matrix, (3) fine crystallite sizes, and (3) high

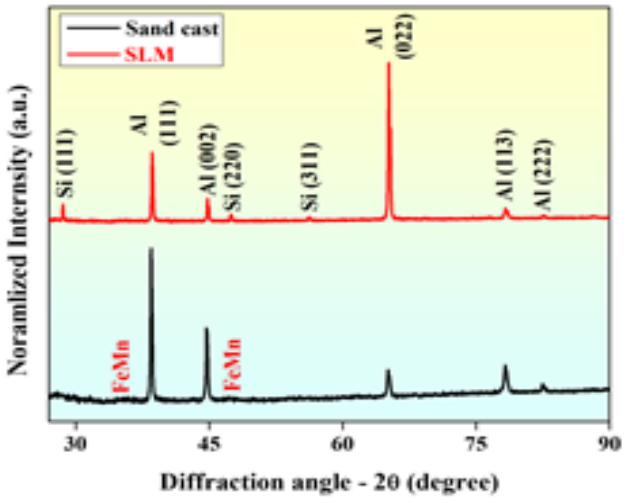

Figure 3. The X-ray diffraction patterns for the AlSi10Mg alloy fabricated through the sand-casting and selective laser melting routes.

degree of defect concentration, especially dislocation density, and stacking faults. The dislocation density of the AlSi10Mg sample processed by SLM (3×10^{15} m/m^3) is three orders of magnitude higher than the SC AlSi10Mg alloy (6×10^{12} m/m^3), which is typical for SLM-processed materials[8,68]. The crystallite size of Al is observed to be 122 nm and 268 nm for the AlSi10Mg fabricated by SLM and SC, respectively. At the same time, the lattice parameters for Al in the Al10SiMg alloy fabricated by SC and SLM routes are found to be 0.40521 nm and 0.40513 nm respectively, which also gives information about the peak positioning that comes from the supersaturation levels observed in the Al lattice[44,68].

3.3 Mechanical Properties

The mechanical properties of the AlSi10Mg samples are tested using a Vickers hardness tester. The SC sample shows a hardness of 35 HV, whereas the SLM samples show a hardness of 135 HV, which is to the published literature[44,69]. Such huge differences in the mechanical properties (like hardness) between the SLM and the SC alloy may be attributed to the following: (1) The presence of a fine microstructure in the SLM samples as compared to the SC counterpart, (2) the presence of a supersaturated solid solution in the SLM processed AlSi10Mg sample, (3) presence of a high degree of internal defects like dislocations in the SLM-fabricated AlSi10Mg, (4) presence of unique microstructural distribution in the SLM-processed samples as compared to the SC ones, and (5) the morphology of Si present along with their length scale.

3.4 Corrosion Properties

Figure 4 and Table 2 show the electrochemical analysis of the AlSi10Mg fabricated by both SC and SLM in the form of PDP curves and Tafel extrapolation plots respectively. The findings of this work from PDP analysis show that the corrosion resistance of both the SLM-fabricated and the SC counterparts are almost similar. From the Tafel plot, it may be observed that the corrosion potential (E_{corr}) for the SLM-fabricated AlSi10Mg alloy is 20 mV more than that of the SC counterpart. A positive rise in E_{corr} (an indicator of corrosion susceptibility) reveals that the specimens fabricated by SLM show relatively

Table 2. Corrosion parameters evaluated from PDP curves and Tafel extrapolation

Specimen	E_{corr} (V)	I_{corr} (μA/cm²)	CR (mpy)
SLM	-0.76	0.50	0.21
Sand Cast	-0.74	0.63	0.27

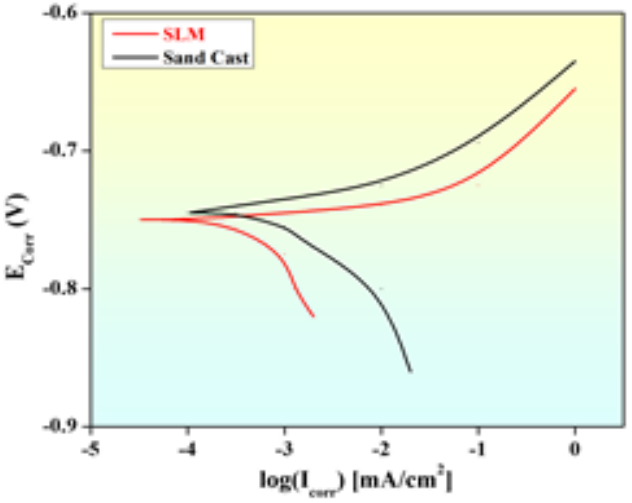

Figure 4. Potentiodynamic polarization curves were observed for the AlSi10Mg samples in 3.5% NaCl solution fabri-cated by sand-casting and selective laser melting process.

improved corrosion resistance than the SC samples. The relatively better corrosion performance of the additively manufactured alloy could be credited significantly to the rapid solidification rate prevalent during the SLM process. The rapid solidification rates observed during SLM help in refining the microstructure, especially the morphology and distribution of the Si. The significant increase in applied voltage results in a rapid rise in the anodic current showing a pitting corrosion behavior, which is more prevalent in the SC AlSi10Mg alloy than in the SLM-fabricated sample, as seen in the anodic side of the Tafel plot in Figure 4. From the PDP curves, it was noted that the SCAlSi10Mg shows higher current densities than the SLM-fabricated alloys, which indicates lower corrosion resistance. This behaviour was also validated from Tafel extrapolation measurements, which show that the corrosion rate of the SLM processed alloy was found to be 0.21 mpy as compared to the SC samples, which is 0.27 mpy. The present results demonstrate that the SLM-processed Al10SiMg shows better corrosion resistance than the SC counterpart when tested in 3.5% NaCl medium unlike most of the published results where mixed properties can be seen.

4. Conclusions

The corrosion properties of the AlSi10Mg samples fabricated by both SC and SLM are evaluated and compared. It has been observed that the corrosion properties of the SLM-fabricated AlSi10Mg alloy show slightly improved resistance as compared to its sand-cast counterpart. The distinct contracts in the microstructural features namely (1) fine microstructural morphology with unique distribution of phases in the SLM samples as compared to the SC counterpart, (2) the presence of a supersaturated solid solution in the SLM processed AlSi10Mg sample, (3) the presence of a high degree of internal defects like dislocations in the SLM-fabricated AlSi10Mg, etc. lead to such difference in the corrosion properties. In addition, the SLM samples also show relatively high hardness as compared to their cast counterpart, suggesting that the SLM process not only produced samples with complex shapes and added functionalities but also can produce samples with improved properties than their cast counterparts.

5. Acknowledgments

This research was funded by Science and Engineering Research Board (A Statutory Body of the Department of Science and Technology), Government of India, under Teachers Associateship for Research Excellence (TARE) Scheme, grant number TAR/2020/000416.

6. References

1. Tofail SAM, Koumoulos EP, Bandyopadhyay A, Bose S, O'Donoghue L, Charitidis C. Additive manufacturing: Scientific and technological challenges, market uptake and opportunities. Mater Today. 2018; 21(1):22-37. https://doi.org/10.1016/j.mattod.2017.07.001
2. Prashanth K, Löber L, Klauss H-J, Kühn U, Eckert J. Characterization of 316L steel cellular dodecahedron structures produced by selective laser melting. Technologies. 2016; 4(4). https://doi.org/10.3390/technologies4040034
3. Ma P, Ji P, Jia Y, Shi X, Yu Z, Prashanth K.G. Effect of substrate plate heating on the microstructure and properties of selective laser melted Al-20Si-5Fe-3Cu-1Mg alloy. Materials. 2021; 14(2). https://doi.org/10.3390/ma14020330
4. Ma P, Jia Y, Prashanth K.G, Scudino S, Yu Z, Eckert J. Microstructure and phase formation in Al-20Si-5Fe-3Cu-1Mg synthesized by selective laser melting. J Alloys Compd. 2016; 657:430-5. https://doi.org/10.1016/j.jallcom.2015.10.119
5. Ma P, Prashanth K, Scudino S, Jia Y, Wang H, Zou C, *et al*. Influence of annealing on mechanical properties of Al-20Si processed by selective laser melting. Metals. 2014; 4(1):28-36. https://doi.org/10.3390/met4010028
6. Ma P, Fan Y, Wei S, Zhang Z, Yang H, Wan S, *et al*. Microstructure and mechanical properties of AlCoCrFeMnNi HEAs fabricated by selective laser melting. J Mater Res Technol. 2023; 25:7090-100. https://doi.org/10.1016/j.jmrt.2023.07.124
7. Jia YD, Zhang LB, Ma P, Scudino S, Wang G, Yi J, *et al*. Thermal expansion behavior of Al–XSi alloys fabricated using selective laser melting. Prog Addit Manuf. 2020; 5(3):247-57. https://link.springer.com/article/10.1007/s40964-020-00130-w
8. Wang Z, Xie M, Li Y, Zhang W, Yang C, Kollo L, *et al*. Premature failure of an additively manufactured material. NPG Asia Materials. 2020; 30. https://doi.org/10.1038/s41427-020-0212-0
9. Wang Z, Tang SY, Scudino S, Ivanov YP, Qu RT, Wang D, *et al*. Additive manufacturing of a martensitic Co–Cr–Mo alloy: Towards circumventing the strength–ductility trade-off. Addit Manuf. 2021; 37. https://doi.org/10.1016/j.addma.2020.101725
10. Zhou X, Li K, Zhang D, Liu X, Ma J, Liu W, *et al*. Textures formed in a CoCrMo alloy by selective laser melting. J Alloys Compd. 2015; 631:153-64. https://doi.org/10.1016/j.jallcom.2015.01.096
11. Prashanth KG, Shahabi HS, Attar H, Srivastava VC, Ellendt N, Uhlenwinkel V, *et al*. Production of high strength Al85Nd8Ni5Co2 alloy by selective laser melting. Addit Manuf. 2015; 6:1–5. https://doi.org/10.1016/j.addma.2015.01.001
12. Lai Z, Guo T, Zhang S, Kollo L, Attar H, Wang Z, *et al*. Selective laser melting of commercially pure silicon. J Wuhan Univ Technol Mater Sci Ed. 2022; 37:1155-65. https://doi.org/10.1007/s11595-022-2647-3
13. Scudino S, Unterdörfer C, Prashanth KG, Attar H, Ellendt N, Uhlenwinkel V, *et al*. additive manufacturing of Cu-10Sn bronze. Mater Lett. 2015; 156:202-4. https://doi.org/10.1016/j.matlet.2015.05.076
14. Attar H, Prashanth KG, Chaubey AK, Calin M, Zhang LC, Scudino S, *et al*. Comparison of wear properties of commercially pure titanium prepared by selective laser melting and casting processes. Mater Lett. 2015; 142:38-41. https://doi.org/10.1016/j.matlet.2014.11.156
15. Attar H, Prashanth KG, Zhang LC, Calin M, Okulov IV, Scudino S, *et al*. Effect of powder particle shape on the properties of *in situ* Ti-TiB composite materials produced by selective laser melting. J Mater Sci Technol. 2015; 31(10): 1001–1005. https://doi.org/10.1016/j.jmst.2015.08.007
16. Singh S, Palani IA, Dehgahi S, Paul CP, Prashanth KG, Qureshi AJ. Influence of the interlayer temperature on structure and properties of CMT wire arc additive manufactured NiTi structures. J Alloys Compd. 2023; 966. https://doi.org/10.1016/j.jallcom.2023.171447
17. Singh S, Palani IA, Paul CP, Funk A, Prashanth KG. Wire arc additive manufacturing of NiTi 4D structures: Influence of interlayer delay. 3D Print Addit Manuf. 2022; 11(1):152-62. https://doi.org/10.1089/3dp.2021.0296
18. Singh N, Hameed P, Ummethala R, Manivasagam G, Prashanth KG, Eckert J. Selective laser manufacturing of Ti-based alloys and composites: Impact of process parameters. Application Trends, and Future Prospects. Mater Today Adv. 2020; 8:100097. https://doi.org/10.1016/j.mtadv.2020.100097
19. Singh N, Edachery V, Rajput M, Chatterjee K, Kailas SV, Prashanth KG. Ti6Al7Nb–TiB nanocomposites for ortho-implant applications. J Mater Res. 2022; 37:2525-2535. https://doi.org/10.1557/s43578-022-00578-2
20. Sokkalingam R, Sivaprasad K, Singh N, Muthupandi V, Ma P, Jia YD, *et al*. Subtle Change in the work hardening behavior of fcc materials processed by selective laser melting. Prog Addit Manuf. 2022; 7:453-61. https://doi.org/10.1007/s40964-022-00301-x

21. Maurya HS, Kollo L, Tarraste M, Juhani K, Sergejev F, Prashanth KG. Selective laser melting of TiC-Fe via Laser pulse shaping: Microstructure and mechanical properties. 3D Print Addit Manuf. 2021; 10(4):640-9. https://doi.org/10.1089/3dp.2021.0221
22. Ummethala R, Jayaraj J, Karamched PS, Rathinavelu S, Singh N, Surreddi KB, *et al*. *In vitro* corrosion behavior of selective laser melted Ti-35Nb-7Zr-5Ta. J Mater Eng Perform. 2021; 30:7967-78. https://doi.org/10.1007/s11665-021-05940-9
23. Hameed P, Liu CF, Ummethala R, Singh N, Huang HH, Manivasagam G, *et al*. Biomorphic porous Ti6Al4V gyroid scaffolds for bone implant applications fabricated by selective laser melting. Prog Addit Manuf. 2021; 6:455-69. https://doi.org/10.1007/s40964-021-00210-5
24. Singh S, Jinoop AN, Palani IA, Paul CP, Tomar KP, Prashanth KG. Microstructure and mechanical properties of NiTi-SS bimetallic structures built using wire arc additive manufacturing. Mater Lett. 2021; 303. https://doi.org/10.1016/j.matlet.2021.130499
25. Ummethala R, Karamched PS, Rathinavelu S, Singh N, Aggarwal A, Sun K, *et al*. Selective laser melting of high-strength, low-modulus Ti–35Nb–7Zr–5Ta alloy. Materialia. 2020; 14. https://doi.org/10.1016/j.mtla.2020.100941
26. Jung HY, Choi SJ, Prashanth KG, Stoica M, Scudino S, Yi S, *et al*. Fabrication of Fe-based bulk metallic glass by selective laser melting: A parameter study. Mater Des. 2015; 86:703-8. https://doi.org/10.1016/j.matdes.2015.07.145
27. Pauly S, Löber L, Petters R, Stoica M, Scudino S, Kühn U, *et al*. Processing metallic glasses by selective laser melting. Mater Today. 2013; 16(1-2): 37-41. https://doi.org/10.1016/j.mattod.2013.01.018
28. Prashanth KG, Scudino S. Quasicrystalline composites by additive manufacturing. Key Eng Mater. 2019; 818:72-6. https://doi.org/10.4028/www.scientific.net/KEM.818.72
29. Karimi J, Kollo L, Prashanth KG. Characterization of gas-atomized equiatomic AlCoCrFeNi powder for additive manufacturing. Metall Mater Trans A. 2023; 54:3417-24. https://doi.org/10.1007/s11661-023-07129-2
30. Karimi J, Antonov M, Prashanth KG. Effect of wear debris entrapment on the tribological performance of AlCoCrFeNi produced by selective laser melting or spark plasma sintering. Metall Mater Trans A. 2022; 53:4004-10. https://doi.org/10.1007/s11661-022-06805-z
31. Karimi J, Suryanarayana C, Okulov I, Prashanth KG. Selective laser melting of Ti6Al4V: Effect of laser re-melting. Mater Sci Eng A. 2021; 805. https://doi.org/10.1016/j.msea.2020.140558
32. Prashanth KG. Processing of Al-based composite material by selective laser melting: A perspective. Mater Today Proc. 2022; 57(2):498-504. https://doi.org/10.1016/j.matpr.2022.01.391
33. Xi L, Gu D, Guo S, Wang R, Ding K, Prashanth KG. Grain refinement in laser manufactured Al-based composites with TiB2 ceramic. J Mater Res Technol. 2020; 9(3):2611-22. https://doi.org/10.1016/j.jmrt.2020.04.059.
34. Wang P, Eckert J, Prashanth KG, Wu M-w, Kaban I, Xi L, *et al*. A review of particulate-reinforced aluminum matrix composites fabricated by selective laser melting. Trans Nonferrous Met Soc China. 2020; 30(8):2001-34. https://doi.org/10.1016/S1003-6326(20)65357-2
35. Xi L, Feng L, Gu D, Wang R, Sarac B, Prashanth KG, *et al*. ZrC+TiC synergically reinforced metal matrix composites with micro/nanoscale reinforcements prepared by laser powder bed fusion. J Mater Res Technol. 2022; 19:4645-57. https://doi.org/10.1016/j.jmrt.2022.06.149
36. Xi L, Xu J, Gu D, Feng L, Lu Q, Prashanth KG. A novel crack-free and refined 2195-Ti/CeB6 composites prepared by laser powder bed fusion. Mater Lett. 2023; 333. https://doi.org/10.1016/j.matlet.2022.133572
37. Yap CY, Chua CK, Dong ZL, Liu ZH, Zhang DQ, Loh LE, *et al*. Review of selective laser melting: Materials and applications. Appl Phys Rev. 2015; 2(4). https://doi.org/10.1063/1.4935926
38. Yu WH, Sing SL, Chua CK, Kuo CN, Tian XL. Particle-reinforced metal matrix nanocomposites fabricated by selective laser melting: A state of the art review. Prog Mater Sci. 2019; 104:330-79. https://doi.org/10.1016/j.pmatsci.2019.04.006
39. Aboulkhair NT, Simonelli M, Parry L, Ashcroft I, Tuck C, Hague R. 3D printing of aluminium alloys: Additive manufacturing of aluminium alloys using selective laser melting. Prog Mater Sci. 2019; 106. https://doi.org/10.1016/j.pmatsci.2019.100578
40. Gharbi O, Jiang D, Feenstra DR, Kairy SK, Wu Y, Hutchinson CR, *et al*. On the corrosion of additively manufactured aluminium alloy AA2024 prepared by selective laser melting. Corros Sci. 2018; 143:93-106. https://doi.org/10.1016/j.corsci.2018.08.019
41. Leon A, Shirizly A, Aghion E. Corrosion behavior of AlSi10Mg alloy produced by Additive Manufacturing (AM) vs. its counterpart gravity cast alloy. Metals. 2016; 6(7). https://doi.org/10.3390/met6070148

42. Revilla RI, Liang J, Godet S, De Graeve I. Local corrosion behavior of additive manufactured AlSiMg alloy assessed by SEM and SKPFM. J Electrochem Soc. 2017; 164(2):C27-35. https://doi.org/10.1149/2.0461702jes
43. Prashanth KG, Debalina B, Wang Z, Gostin PF, Gebert A, Calin M, Kühn U, *et al*. Tribological and corrosion properties of Al-12Si produced by selective laser melting. J Mater Res. 2014; 29:2044-54. https://doi.org/10.1557/jmr.2014.133
44. Prashanth KG, Scudino S, Klauss HJ, Surreddi KB, Löber L, Wang Z, *et al*. Microstructure and mechanical properties of Al-12Si produced by selective laser melting: Effect of heat treatment. Mater Sci Eng A. 2014; 590: 153-60. https://doi.org/10.1016/j.msea.2013.10.023
45. Wang Z, Ummethala R, Singh N, Tang S, Suryanarayana C, Eckert J, *et al*. Selective laser melting of aluminum and its alloys. Materials. 2020; 13(20). https://doi.org/10.3390/ma13204564
46. Liao H, Wu Y, Zhou K, Yang J. Hot deformation behavior and processing map of Al–Si–Mg alloys containing different amount of silicon based on Gleebe-3500 hot compression simulation. Mater Des. 2015; 65:1091-9. https://doi.org/10.1016/j.matdes.2014.08.021
47. Lin YC, Luo SC, Huang J, Yin LX, Jiang XY. Effects of solution treatment on microstructures and micro-hardness of a sr-modified Al-Si-Mg Alloy. Mater Sci Eng A. 2018; 725:530-40. https://doi.org/10.1016/j.msea.2018.04.049
48. Read N, Wang W, Essa K, Attallah MM. Selective laser melting of AlSi10Mg alloy: Process optimisation and mechanical properties development. Mater Des. 2015; 65:417-24. https://doi.org/10.1016/j.matdes.2014.09.044
49. McDonald SD, Nogita K, Dahle AK. Eutectic nucleation in Al–Si alloys. Acta Mater. 2004; 52(14):4273-80. https://doi.org/10.1016/j.actamat.2004.05.043
50. Jung JG, Lee SH, Lee JM, Cho YH, Kim SH, Yoon WH. Improved mechanical properties of near-eutectic Al-Si piston alloy through ultrasonic melt treatment. Mater Sci Eng A. 2016; 669:187-95. https://doi.org/10.1016/j.msea.2016.05.087
51. Ravi KR, Manivannan S, Phanikumar G, Murty BS, Sundarraj S. Influence of Mg on grain refinement of near eutectic Al-Si alloys. Metall Mater Trans A. 2011; 42:2028-39. https://doi.org/10.1007/s11661-010-0600-0
52. Prashanth KG, Eckert J. Formation of metastable cellular microstructures in selective laser melted alloys. J Alloys Compd. 2017; 707:27-34. https://doi.org/10.1016/j.jallcom.2016.12.209
53. Prashanth KG, Scudino S, Chaubey AK, Löber L, Wang P, *et al*. Processing of Al-12Si-TNM composites by selective laser melting and evaluation of compressive and wear properties. J Mater Res. 2016; 31:55-65. https://doi.org/10.1557/jmr.2015.326
54. Zhao C, Wang Z, Li D, Kollo L, Luo Z, Zhang W, *et al*. Cu-Ni-Sn alloy fabricated by melt spinning and selective laser melting: A comparative study on the microstructure and formation kinetics. J Mater Res Technol. 2020; 9(6):13097-105. https://doi.org/10.1016/j.jmrt.2020.09.047
55. Wu J, Wang XQ, Wang W, Attallah MM, Loretto MH. Microstructure and strength of selectively laser melted AlSi10Mg. Acta Mater. 2016; 117:311-20. https://doi.org/10.1016/j.actamat.2016.07.012
56. Pezzato L, Dabalà M, Gross S, Brunelli K. Effect of microstructure and porosity of AlSi10Mg alloy produced by selective laser melting on the corrosion properties of plasma electrolytic oxidation coatings. Surf Coat Int. 2020; 404. https://doi.org/10.1016/j.surfcoat.2020.126477
57. Chen H, Zhang C, Jia D, Wellmann D, Liu W. Corrosion behaviors of selective laser melted aluminum alloys: A review. Metals. 2020; 10(1). https://doi.org/10.3390/met10010102
58. Cabrini M, Lorenzi S, Pastore T, Testa C, Manfredi D, Lorusso M, *et al*. Corrosion behavior of AlSi10Mg alloy produced by laser powder bed fusion under chloride exposure. Corros Sci. 2019; 152:101-8. https://doi.org/10.1016/j.corsci.2019.03.010
59. Rafieazad M, Mohammadi M, Gerlich A, Nasiri A. Enhancing the corrosion properties of additively manufactured AlSi10Mg using friction stir processing. Corros Sci. 2021; 178. https://doi.org/10.1016/j.corsci.2020.109073
60. De Damborenea J, Conde A, Gardon M, Ravi GA, Arenas MA. Effect of growth orientation and heat treatment on the corrosion properties of AlSi10Mg alloy produced by additive manufacturing. J Mater Res Technol. 2022; 18: 5325-36. https://doi.org/10.1016/j.jmrt.2022.05.021
61. Zakay A, Aghion E. Effect of post-heat treatment on the corrosion behavior of AlSi10Mg alloy produced by additive manufacturing. The Journal of the Minerals, Metals and Materials Society. 2019; 71:1150-7. https://doi.org/10.1007/s11837-018-3298-x
62. Kubacki GW, Brownhill JP, Kelly RG. Comparison of atmospheric corrosion of additively manufactured and cast Al-10Si-Mg over a range of heat treatments.

Corrosion. 2019; 75(12):1527-40. https://doi.org/10.5006/3318
63. Gu XH, Zhang JX, Fan XL, Zhang LC. Corrosion behavior of selective laser melted AlSi10Mg alloy in NaCl solution and its dependence on heat treatment. Acta Metall Sin. 2020; 33:327-37. https://doi.org/10.1007/s40195-019-00903-5
64. Örnek C. Additive manufacturing – a general corrosion perspective. Corros Eng Sci Technol. 2018; 53(7): 531-5. https://doi.org/10.1080/1478422X.2018.1511327
65. Song J, Chew Y, Jiao L, Yao X, Moon SK, Bi G. Numerical study of temperature and cooling rate in selective laser melting with functionally graded support structures. Additive manufacturing. 2018; 24:543-51. https://doi.org/10.1016/j.addma.2018.10.039
66. Wang P, Deng L, Prashanth KG, Pauly S, Eckert J, Scudino S. Microstructure and mechanical properties of Al-Cu alloys fabricated by selective laser melting of powder mixtures. J Alloys Compd. 2018; 735:2263-6. https://doi.org/10.1016/j.jallcom.2017.10.168
67. Gustmann T, Neves A, Kühn U, Gargarella P, Kiminami CS, Bolfarini C, *et al*. Influence of processing parameters on the fabrication of a Cu-Al-Ni-Mn shape-memory alloy by selective laser melting. Addit Manuf. 2016; 11:23-31. https://doi.org/10.1016/j.addma.2016.04.003
68. Prashanth KG, Damodaram R, Scudino S, Wang Z, Rao KP, Eckert J. Friction welding of Al-12Si parts produced by selective laser melting. Mater Des. 2014; 57:632-7. https://doi.org/10.1016/j.matdes.2014.01.026
69. Prashanth K.G, Scudino S, Eckert J. Defining the tensile properties of Al-12Si parts produced by selective laser melting. Acta Mater. 2017; 126:25-35. https://doi.org/10.1016/j.actamat.2016.12.044